Detecting the rise and fall of the first stars by their impact on cosmic reionization

Article (Published Version)

Detecting the Rise and Fall of the First Stars by Their Impact on Cosmic Reionization

Kyungjin Ahn[1]

Ilian T. Iliev[2]

Paul R. Shapiro[3]

Garrelt Mellema[4]

Jun Koda[5]
and

Yi Mao[3]

ABSTRACT

The intergalactic medium was reionized before redshift $z \sim 6$, most likely by starlight which escaped from early galaxies. The very first stars formed when hydrogen molecules (H_2) cooled gas inside the smallest galaxies, *minihalos* of mass between 10^5 and 10^8 solar masses, before redshift $z \sim 40$. Minihalo stars then started reionization but could not finish it before the rising background of H_2-dissociating soft-ultraviolet starlight choked them off. We confirm this hypothesis by the first large-scale radiative transfer simulations to include minihalo sources and their suppression. We show that reionization began much earlier *with* minihalo sources than without, and was greatly extended, which boosts the intergalactic electron-scattering optical depth and the large-angle polarization fluctuations of the cosmic microwave background significantly. Although within current *WMAP* uncertainties, this boost should be readily detectable by *Planck*. If reionization ended as late as $z_{\rm ov} \lesssim 7$, as suggested by other observations, *Planck* will thereby see the signature of the first stars at high redshift, currently undetectable by any other probe. We also show that minimal reionization models satisfying both the late reionization condition, $z_{\rm ov} \lesssim 7$, and the large optical depth condition, $\tau_{\rm es} \gtrsim 0.085$, can be distinguished from our fiducial model under the same constraints by *Planck* at high confidence level.

Subject headings: cosmology: theory — galaxies: high-redshift — radiative transfer

[1]Department of Earth Sciences, Chosun University, Gwangju 501-759, Korea; kjahn@chosun.ac.kr

[2]Astronomy Centre, Department of Physics & Astronomy, Pevensey II Building, University of Sussex, Falmer, Brighton BN1 9QH, United Kingdom

[3]Department of Astronomy, University of Texas, Austin, TX 78712-1083, U.S.A

[4]Department of Astronomy & Oskar Klein Centre, Stockholm University, Albanova, SE-10691 Stockholm, Sweden

[5]Centre for Astrophysics & Supercomputing, Swinburne University of Technology, Hawthorn, Victoria 3122, Aus-

1. Introduction

The theory of reionization has not yet advanced to the point of establishing unambiguously its timing and the relative contributions to it from galaxies of different masses. In the Cold Dark Matter ("CDM") universe, these early galactic sources can be grouped broadly by their host dark-matter halo mass into two categories: minihalos ("MHs") and "atomic-cooling" halos ("ACHs"). MHs have masses between $\sim 10^5$ and $\sim 10^8$ $M_\odot$ (solar masses) and virial temperatures below $\sim 10^4$ K, in which molecular hydrogen (H_2) was necessary to cool the gas below this virial temperature to begin star formation. ACHs have masses above $\sim 10^8$ $M_\odot$ and virial temperatures $\gtrsim 10^4$ K, for which H-atom radiative line cooling alone was sufficient. The ACHs can be split further into low-mass atomic-cooling halos ("LMACHs"; masses between $\sim 10^8$ and $\sim 10^9$ $M_\odot$), for which the gas pressure of the photoionization-heated intergalactic medium ("IGM") in an ionized patch prevented the halo from capturing the gas it needed to form stars, and high-mass atomic-cooling halos ("HMACHs"; masses above $\sim 10^9$ $M_\odot$), for which gravity was strong enough to overcome this "Jeans-mass filter" and form stars even in the ionized patches.

Once starlight escaped from galactic halos into the IGM to reionize it, the ionized patches ("H II regions") of the IGM were places in which both MHs and LMACHs were suppressed. At the same time, UV starlight at energies in the range 11.2 – 13.6 eV also escaped from the halos, capable of destroying the H_2 molecules inside MHs through Lyman-Werner band ("LW") dissociation, even in the neutral zones of the IGM. This dissociation eventually prevented further star formation wherever the background intensity was high enough.

We report the first radiative transfer simulations of reionization to include *all three* of the mass categories of reionization source halos, along with their radiative suppression, in a simulation volume large enough to capture both the global mean ionization history and the observable consequences of its evolving patchiness in a statistically meaningful way. We overcame the limitation of previous large-volume simulations by applying a newly developed sub-grid treatment to include minihalo sources (section 2), and also calculated the transfer of LW-band radiation using the scheme by Ahn et al. (2009).

tralia

2. Methods

We performed a cosmological N-body simulation of structure formation with 3072^3 particles in a $114/h$ Mpc simulation box, using the WMAP5 background cosmology (Dunkley et al. 2009). For this we used the code CubeP^{3}M (Merz et al. 2005; Iliev et al. 2008), in which the gravity is computed by a P^{3}M (particle-particle-particle-mesh) scheme. The simulation was started at redshift $z = 300$ and run to $z = 6$. N-body data (particle position and velocity) were recorded at 86 equally-spaced times (every 11.53 Myrs) from $z = 50$ to $z = 6$. Each data time-slice was then used to create matter density fields by smoothing the particle data adaptively onto a uniform mesh – or a "radiative transfer grid" – of 256^3 cells. All cosmological haloes with masses 10^8 $M_\odot$ or above (corresponding to 20 particles or more), and thus both LMACHs and HMACHs, were identified on-the-fly using a spherical overdensity halo finder with overdensity of $\Delta = 178$.

Unlike LMACHs and HMACHs, the minihalos are too small to be resolved in our simulation box, and thus our radiative transfer grid was populated with minihalos by means of a newly-developed sub-grid model, as follows. We started with a separate, high-resolution N-body simulation of structure formation in a comoving box with $(6.3/h$ Mpc$)^3$ volume and 1728^3 particles, which resolved all minihalos with mass $M \geq 10^5 M_\odot$ with 20 particles or more. We then partitioned the box into a uniform grid of 14^3 cells, such that each cell is the same size as one of the radiative transfer grid cells in our main, $114/h$ Mpc simulation box, and calculated the total number of minihalos per cell and the cell density. Our results, shown in Fig. 1, indicate a strong and fairly tight correlation between the number of minihalos located in a cell and its density. The best fit to this correlation at each redshift was then used to populate each grid cell in our $114/h$ Mpc box with minihalos based on its density at each given time-slice.

Based on these structure formation results for the IGM density field and the source galactic

haloes, we then calculated the radiative transfer (RT) of H-ionizing and H_2-dissociating photons. The stars inside the ACHs are assumed to produce g_γ ionizing photons per baryon every 10 Myrs, where $g_\gamma \equiv f_\gamma/(t_\star/10\,\mathrm{Myr})$, and where $f_\gamma \equiv f_\mathrm{e} f_\star N_\mathrm{i}$, f_e is the escape fraction of ionizing photons, $f_\star$ is the star formation efficiency (i.e. the fraction of the halo baryonic mass which forms stars), and N_i is the number of ionizing photons per stellar baryon produced over the star's lifetime $t_\star$ – we use $t_\star = 11.53\,\mathrm{Myr}$ for both HMACHs and LMACHs, and $t_\star = 1.92\,\mathrm{Myr}$ for MHs. We assign one Pop III star per minihalo, motivated by numerical simulations of first-star formation inside minihaloes, which find that typically one Pop III star with a mass between 100 and $1000\,M_\odot$ forms per minihalo in the absence of strong soft UV radiative feedback (Yoshida et al. 2006; Bromm et al. 2002; Abel et al. 2002). Star formation in minihaloes is suppressed when the local LW background – calculated at each time step using the scheme by Ahn et al. (2009), but now considering both ACHs and minihalos and also improved in speed using the fast Fourier transform (FFT) scheme – reaches a certain threshold $J_{\mathrm{LW,\,th}}$. At present the precise value of this threshold is not well determined, but the typical values found by high-resolution simulations of minihalo star formation are $J_{\mathrm{LW,\,th}} = [0.01-0.1]\times 10^{-21}\,\mathrm{erg\,s^{-1}\,cm^{-2}\,sr^{-1}}$ (Machacek et al. 2001; Yoshida et al. 2003; O'Shea & Norman 2008). We adopted a constant value chosen from this range for each simulation.

The simulations with ACHs only (and without LW radiative transfer) are described in Iliev et al. (2012). Simulation parameters are described in Table 1.

3. Role of the first stars during cosmic reionization

We demonstrate the effects of the first stars by direct comparison of the results from two simulations, a fiducial case which includes all ionizing sources down to the first stars hosted by minihalos (Case L2M1) and a corresponding reference case which includes the larger, atomically-cooling halos with exactly the same properties, but no minihalo sources (Case L2, previously presented in ref. Iliev et al. (2012)). Our results show that the early reionization history was completely dominated by the first stars, while the late (redshift $z \lesssim 10$) history was driven by the stars inside HMACHs (Figs 2A and 2C, top panel). The very first stars started to form inside MHs at redshift $z \simeq 40$ (when the age of the universe was just 70 Myrs), and dominated the reionization process until $z \simeq 10$. Although the abundance of more massive halos, the ACHs, rose exponentially, they remained relatively rare, and thus sub-dominant, until $z \simeq 10$. After redshift $z \simeq 8$, though, the two reionization histories became largely indistinguishable, because the same HMACHs then dominated reionization. Before that, however, the mean intensity J_LW of the LW background produced by MH stars (see Figs 2B and 2C, bottom panel) rose, on average, to $J_{\mathrm{LW,\,th}}$, the threshold level above which H_2 is dissociated and star formation suppressed inside MHs, as early as $z \simeq 23$ – locally, $J_{\mathrm{LW,\,th}}$ was reached even earlier, as early as $z \simeq 30$, due to inhomogeneities in the background (Fig. 2B). Thereafter, MH star formation continued but was self-regulated, which slowed their contribution to reionization until the ACHs finally rose up to push J_LW *above* $J_{\mathrm{LW,\,th}}$ (at $z \simeq 12$), halting MH star formation altogether, long before the MHs could complete reionization on their own.

Nonetheless, the minihalo sources (the first stars) did have quite a dramatic effect on the electron-scattering optical depth τ_es. While intergalactic H II regions fully overlapped (at redshift z_ov, defined as the epoch when the mean ionized fraction by mass, x_m, first surpassed 99%) at almost identical redshifts, $z_\mathrm{ov} \simeq 6.8$, with (L2M1) or without (L2) minihalos, the early rise of x_m with minihalo sources boosted the optical depth by as much as 47 % relative to that without minihalo sources: $\tau_\mathrm{es} = 0.0861$ in case L2M1, while $\tau_\mathrm{es} = 0.0603$ in case L2. This satisfies the current observational constraints on reionization: (1) reionization ended no earlier than redshift $z = 7$ (Fan & et al. 2006; Mortlock et al. 2011; Bolton et al. 2011; Pentericci et al. 2011; Ota et al. 2010)), and (2) $\tau_\mathrm{es} = 0.088 \pm 0.015$ at 68 % confidence level (Larson et al. 2011). Predicted values of τ_es and z_ov are model-dependent, and thus we tested the robustness of our conclusions by varying the physical parameters of MHs and ACHs.

The first stars, born inside MHs, imprinted a distinctive pattern on the global reionization his-

tory. For example, in case L2M1, when the LW-plateau ended, reionization briefly stalled, since MHs no longer formed the stars which replenished the ionizing background and only ACH sources remained, thereafter; the ACH contribution took a bit more time to climb enough to move reionization forward again. This explains the brief "x_m-plateau" from $z \sim 12$ to $z \sim 10$ in Fig. 2C for case L2M1, while in case L2, x_m grew continuously without showing such a plateau (Fig. 2C). This feature is generic (Figs 3 and 4B): without minihalos, the universe underwent a monotonic and rapid increase in x_m. Reionization histories *without* MH sources, modelled either by large-scale radiative transfer simulations (Ciardi et al. 2003; Iliev et al. 2007; Trac & Cen 2007; Iliev et al. 2012; Iliev et al. 2006; McQuinn et al. 2007; Zahn et al. 2007) or semi-analytical calculations (Zahn et al. 2007; Haiman et al. 2000), are all similar in that respect. Reionization histories *with* MH sources, however, calculated here for the first time by large-scale N-body + radiative transfer simulations that take account of radiative suppression by both photoionization and LW dissociation, find an ionization plateau phase. Previous studies that considered MH stars and their impact were not able to settle the issue of their global effect on reionization, either because they simulated volumes much too small to represent a fair portion of the Universe (Ricotti et al. 2002; Yoshida et al. 2006; Ricotti et al. 2008), or else treated reionization by a semi-analytical, 1-zone, homogeneous approximation (either *with* LW suppression included (Haiman et al. 2000; Furlanetto & Loeb 2005) or *without* (Haiman & Bryan 2006; Wyithe & Loeb 2003; Wyithe & Cen 2007; Shapiro et al. 1994)), which cannot capture its innate spatially inhomogeneous nature, or made a semi-analytical approximation that accounted statistically for spatial inhomogeneity but without LW suppression (Kramer et al. 2006).

4. Probing the first stars with *Planck*

The first stars hosted by minihalos likely made an important contribution to reionization. But how can we probe them observationally? While significant, the effects of the first stars are largely confined to the early stages of reionization, at redshifts $z > 10$, which puts them beyond the reach of most current instruments. Future, very sensitive experiments like the Square Kilometre Array (SKA) and the James Webb Space Telescope (JWST) may be able to probe these distant epochs directly. However, we have shown above that the combined effect of the first stars also considerably increases the value of the integrated electron scattering optical depth $\tau_{\rm es}$ compared to reionization scenarios in which the first stars are absent. Different values of $\tau_{\rm es}$ are clearly reflected in the cosmic microwave background (CMB) polarization anisotropies at large scales. The current best constraints on $\tau_{\rm es}$ by the *WMAP* satellite $\tau_{\rm es}$ are still relatively weak, and thus models with low-$\tau_{\rm es}$ values like L2 are still acceptable at the 2σ (95%) confidence level (Fig. 2C, middle panel). By contrast, the current *Planck* mission, which will measure the CMB polarization far more precisely than *WMAP*, should already be able to discern the influence of the first stars on reionization. In Fig. 4A we show our forecasts for the angular spectra of CMB E-mode autocorrelation (EE).

As we discussed above, current observational constraints strongly suggest that reionization was not complete before redshift $z \sim 7$. Imposing this condition as a prior on the allowed reionization histories $x_m(z)$, we predict that the *Planck* mission will clearly and unambiguously detect the era of first stars. In Fig. 4B we show a statistical measure of the *Planck* sensitivity to detecting the signature of the first stars using "principal-component amplitudes" $\{m_\mu\}$ following Mortonson & Hu (2008)[1], we experimented for the details of the principal component analysis of reionization models. Based on the *Planck* data after its full 2 years of planned operation, the narrow posterior distribution of allowed $\tau_{\rm es}$ values will allow us to distinguish reionization models like L2 and L2M1 *unambiguously*, and thereby strongly constrain the available reionization parameter space. A high measured measured value of $\tau_{\rm es} > 0.085$ will be a clear (if indirect) signature of the first stars.

Finally, we note that the presence of these first stars in cosmological minihalos introduces certain unique features in the reionization history, like the plateau noted above, which in turn show up

[1]While we use the scheme developed by Mortonson & Hu (2008), we implemented the following ingredients in order to optimize the analysis for our purpose. First, to apply the late-reionization prior, $z_{\rm ov} \leq 7$

as characteristic features in the CMB polarization power spectrum. Hence, *Planck* might be able to distinguish (albeit at lower statistical significance, of $\gtrsim 2\sigma$ or $\gtrsim 95\%$) reionization models with and without first stars *even* if they have very similar values of $\tau_{\rm es}$ and similar end-of-reionization redshifts $z_{\rm ov}$ (Fig. 4). Full reionization simulations like ours find it hard to satisfy both of these observational constraints without including a significant contribution from the first stars, but some semi-analytical models (Haiman & Bryan 2006; Haardt & Madau 2012) do find such scenarios. However, all such models lack the plateau feature in the reionization history $x_m(z)$, and thus reside in a narrow window of m_μ-parameter space adjacent to that occupied by our no-minihalo cases, as demonstrated in Fig. 4B.

In summary, *Planck* is capable of distinguishing with high confidence between definitive classes of reionization scenarios allowed by the current constraints, and thereby significantly restricting the available parameter space. *Planck* will either probe the signature of the first stars, or show that the first stars had a negligible impact on reionizaion. Once these first results confirm the role of the first stars, simulation modelling like that presented here can be used to guide and understand further, more detailed theoretical and observational studies of the early universe.

K.A. was supported in part by NRF grant funded by the Korean government MEST (No. 2009-0068141, 2009-0076868, 2012-014646). ITI was supported by The Southeast Physics Network (SEPNet) and the Science and Technology Facilities Council grants ST/F002858/1 and ST/I000976/1. This study was supported in part by the Swedish Research Council grant 2009-4088, U.S. NSF grants AST-0708176 and AST-1009799, NASA grants NNX07AH09G, NNG04G177G and NNX11AE09G, and Chandra grant SAO TM8-9009X. The authors acknowledge the TeraGrid and the Texas Advanced Computing Center (TACC) at The University of Texas at Austin (URL: http://www.tacc.utexas.edu), as well as the Swedish National Infrastructure for Computing (SNIC) resources at HPC2N (Umeå, Sweden) for providing HPC and visualization resources that have contributed to the research results reported within this paper. We acknowledge A. Lewis, A. Liddle and M. Mortonson for scientific and technical input on *Planck* forecasts (Lewis, Liddle) and COSMOMC modified for reionization principal components (Mortonson).

REFERENCES

Abel, T., Bryan, G. L., & Norman, M. L. 2002, Science, 295, 93

Ahn, K., Shapiro, P. R., Iliev, I. T., Mellema, G., & Pen, U. 2009, Astrophys. J. , 695, 1430

Bolton, J. S., Haehnelt, M. G., Warren, S. J., Hewett, P. C., Mortlock, D. J., Venemans, B. P., McMahon, R. G., & Simpson, C. 2011, Mon. Not. R. Astron. Soc. , 416, L70

Bromm, V., Coppi, P. S., & Larson, R. B. 2002, Astrophys. J. , 564, 23

Ciardi, B., Stoehr, F., & White, S. D. M. 2003, Mon. Not. R. Astron. Soc. , 343, 1101

Dunkley, J., et al. 2009, Astrophys. J. Suppl., 180, 306

Fan, X., & et al. 2006, Astron. J. , 132, 117

Furlanetto, S. R., & Loeb, A. 2005, Astrophys. J. , 634, 1

Haardt, F., & Madau, P. 2012, Astrophys. J. , 746, 125

Haiman, Z., Abel, T., & Rees, M. J. 2000, Astrophys. J. , 534, 11

Haiman, Z., & Bryan, G. L. 2006, Astrophys. J. , 650, 7

Iliev, I. T., Mellema, G., Pen, U.-L., Merz, H., Shapiro, P. R., & Alvarez, M. A. 2006, Mon. Not. R. Astron. Soc. , 369, 1625

Iliev, I. T., Mellema, G., Shapiro, P. R., & Pen, U. 2007, Mon. Not. R. Astron. Soc. , 376, 534

Iliev, I. T., Mellema, G., Shapiro, P. R., Pen, U.-L., Mao, Y., Koda, J., & Ahn, K. 2012, Mon. Not. R. Astron. Soc. , in press

Iliev, I. T., Shapiro, P. R., Mellema, G., Merz, H., & Pen, U.-L. 2008, in Proceedings of the TeraGrid 2008 Conference. June 9-13, 2008. Las Vegas, USA. ¡A href="http://archive.teragrid.org/events/teragrid08/index.htm"¿ http://archive.teragrid.org/events/teragrid08/index.htm¡/A¿, p.31, 31

Kramer, R. H., Haiman, Z., & Oh, S. P. 2006, Astrophys. J. , 649, 570

Larson, D., et al. 2011, Astrophys. J. Suppl. Ser. , 192, 16

Machacek, M. E., Bryan, G. L., & Abel, T. 2001, Astrophys. J. , 548, 509

McQuinn, M., Lidz, A., Zahn, O., Dutta, S., Hernquist, L., & Zaldarriaga, M. 2007, Mon. Not. R. Astron. Soc. , 377, 1043

Merz, H., Pen, U.-L., & Trac, H. 2005, New Astronomy, 10, 393

Mortlock, D. J., et al. 2011, Nature , 474, 616

Mortonson, M. J., & Hu, W. 2008, Astrophys. J., 672, 737

O'Shea, B. W., & Norman, M. L. 2008, Astrophys. J. , 673, 14

Ota, K., et al. 2010, Astrophys. J. , 722, 803

Pentericci, L., et al. 2011, Astrophys. J. , 743, 132

Ricotti, M., Gnedin, N. Y., & Shull, J. M. 2002, Astrophys. J. , 575, 33

—. 2008, Astrophys. J. , 685, 21

Shapiro, P. R., Giroux, M. L., & Babul, A. 1994, Astrophys. J. , 427, 25

Trac, H., & Cen, R. 2007, Astrophys. J. , 671, 1

Wyithe, J. S. B., & Cen, R. 2007, Astrophys. J. , 659, 890

Wyithe, J. S. B., & Loeb, A. 2003, Astrophys. J. Lett. , 588, L69

Yoshida, N., Abel, T., Hernquist, L., & Sugiyama, N. 2003, Astrophys. J., 592, 645

Yoshida, N., Omukai, K., Hernquist, L., & Abel, T. 2006, Astrophys. J., 652, 6

Zahn, O., Lidz, A., McQuinn, M., Dutta, S., Hernquist, L., Zaldarriaga, M., & Furlanetto, S. R. 2007, Astrophys. J. , 654, 12

This 2-column preprint was prepared with the AAS LaTeX macros v5.2.

Table 1: Reionization simulation source halo properties and global history results. $M_{\rm III,*}$ and $J_{\rm LW,th}$ are in units of solar mass ($M_\odot$) and $10^{-21}\,{\rm erg\,s^{-1}\,cm^{-2}\,sr^{-1}}$, respectively. *Note*: Minihalo efficiencies $g_{\gamma,\rm MH}$ ($f_{\gamma,\rm MH}$) quoted here are for the minimum-mass halo assumed to contribute, $10^5\,M_\odot$, which is roughly comparable to the average value for the minihalos integrated over the halo mass function.

case	$g_{\gamma,\rm H}$ ($f_{\gamma,\rm H}$)	$g_{\gamma,\rm L}$ ($f_{\gamma,\rm L}$)	$g_{\gamma,\rm MH}$ ($f_{\gamma,\rm MH}$)	$M_{\rm III,*}$	$J_{\rm LW,th}$	$z_{\rm ov}$	$\tau_{\rm es}$	$m_1, m_2, ..., m_7$
g8.7_130S (L1)	8.7 (10)	130 (150)	·	·	·	8.40	0.0841	-0.298, -0.0267, 0.289, 0.115, 0.0975, 0.0918, -0.0548
g8.7_130S_M300_J0.05 (L1M1)	8.7 (10)	130 (150)	5063 (1013)	300	0.05	8.41	0.0934	-0.283, -0.0222, 0.268, 0.121, 0.0828, 0.0897, -0.0565
g1.7_8.7S (L2)	1.7 (2)	8.7 (10)	·	·	·	6.76	0.0603	-0.298, 0.00402, 0.372, 0.191, 0.0446, 0.0229, -0.0416
g1.7_8.7S_M300_J0.1 (L2M1)	1.7 (2)	8.7 (10)	5063 (1013)	300	0.1	6.80	0.0861	-0.276, -0.00969, 0.302, 0.158, 0.0260, 0.00619, -0.0349

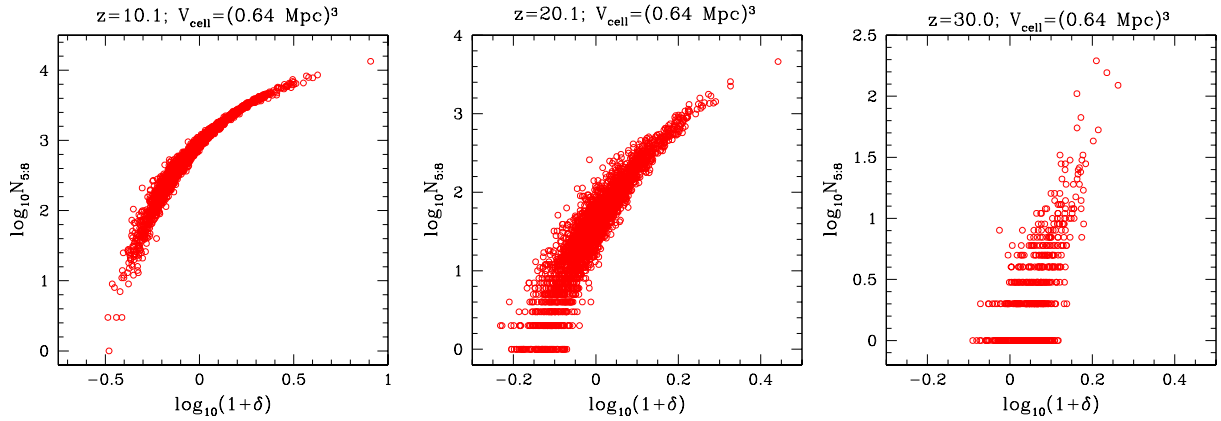

Fig. 1.— Correlation between the total number of minihaloes per RT cell ($N_{5:8}$) and the density of the RT cell in units of the mean density $(1+\delta)$, based on a $6.3/h\,$Mpc box N-body simulation which resolves all haloes with mass $M \geq 10^5\,M_\odot$. Plots are for correlations at three different redshifts, z =30, 20.1 and 10.1 from left to right. The volume occupied by an RT cell is $(0.64{\rm Mpc})^3$. The average correlation at each redshift was used to populate RT cells of the $114/h\,$Mpc box with minihaloes of $10^5 \leq M/M_\odot < 10^8$ at each redshift.

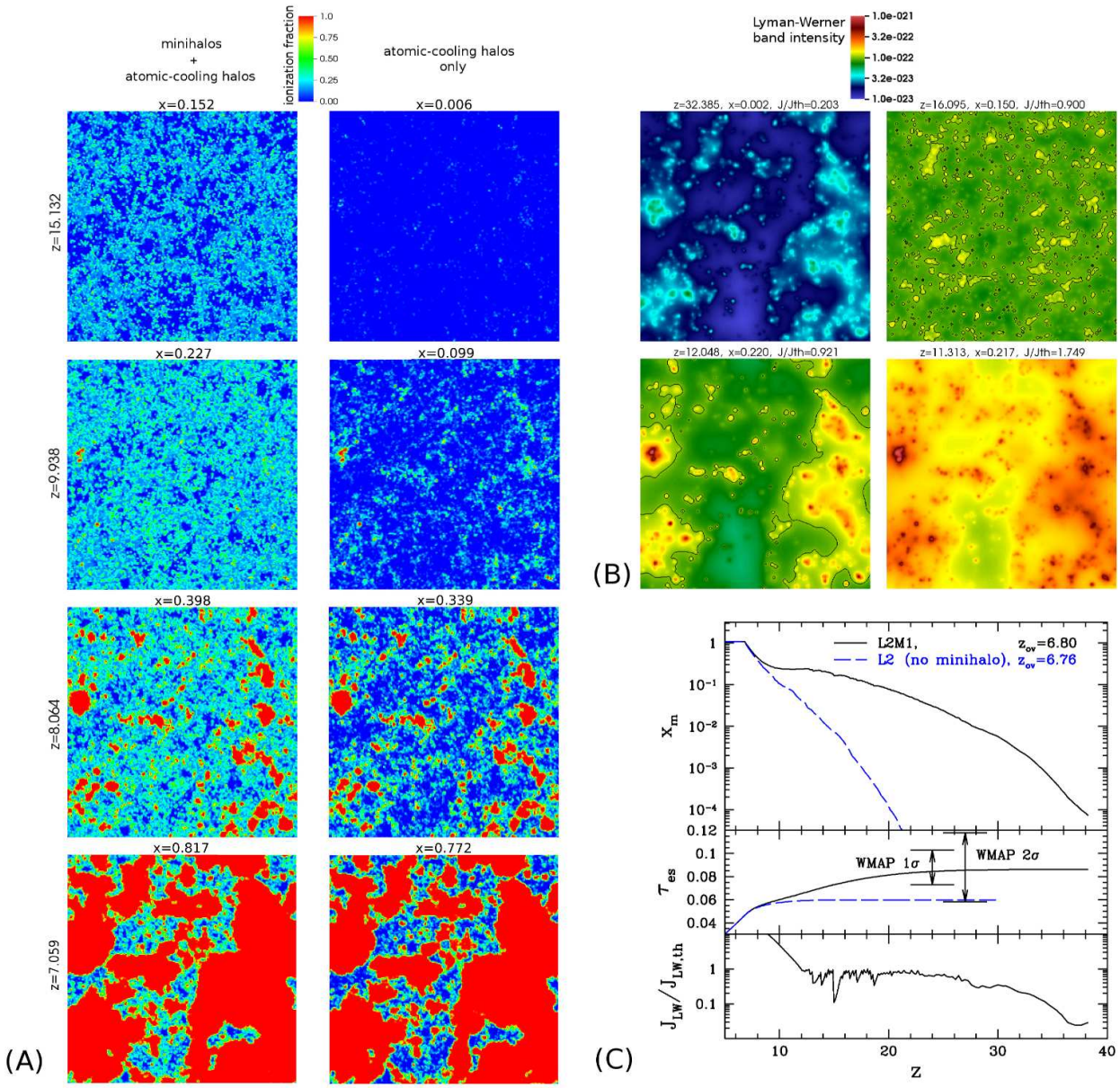

Fig. 2.— (A) Maps of evolving hydrogen-ionized fractions at different redshifts (rows), for our fiducial model with minihalo sources included, L2M1 (1st column), vs. the corresponding reference model with only atomically-cooling halos, case L2 (2nd column). The slices are $0.45/h$ Mpc-thick. Color represents linearly-scaled ionized fraction from 0 (blue) to 1 (red). (B) Maps of evolving Lyman-Werner band intensity for case L2M1. Black contours indicate the threshold value for suppression of star formation, $J_{\rm LW,\,th}$ (which for case L2M1 is set at $0.1 \times 10^{-21}\,{\rm erg\,s^{-1}\,cm^{-2}\,sr^{-1}}$). (C) (top) Globally-averaged history of the mass-weighted ionized fraction for models L2M1 (black, solid) and L2 (blue, dashed). (middle) Thomson scattering optical depth of IGM to CMB integrated from $z = 0$ to redshift z for L2 and L2M1. (bottom) Evolution of the mean LW H_2-dissociating background $J_{\rm LW}$ in units of the threshold value $J_{\rm LW,\,th}$ for Case L2M1.

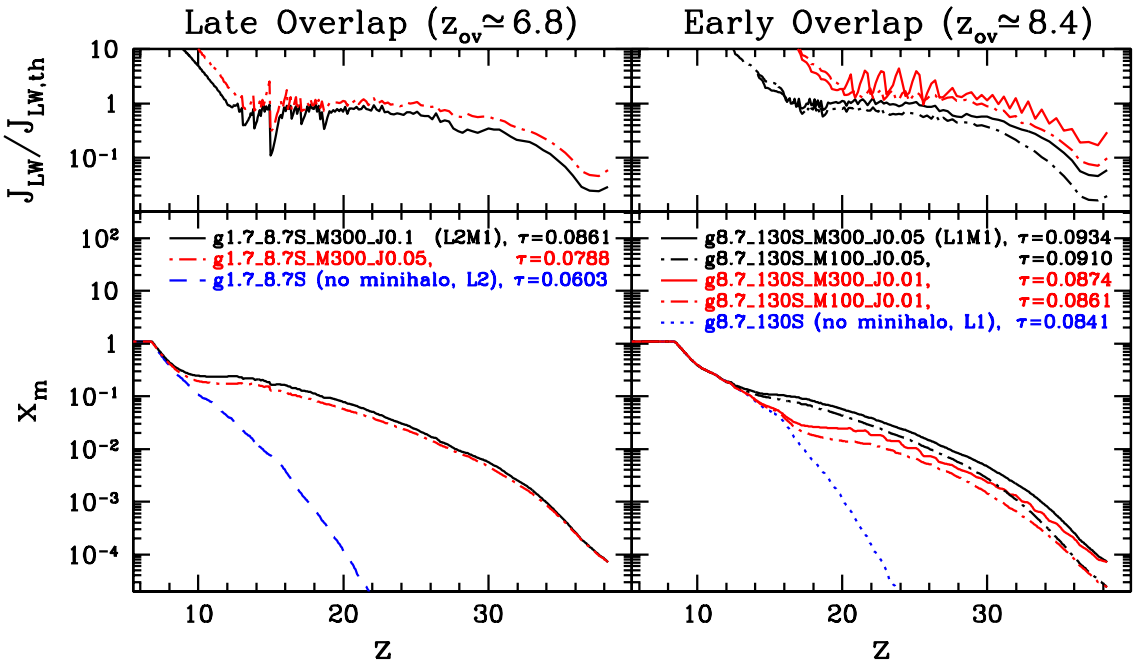

Fig. 3.— Model dependency of the history of cosmic reionization. In addition to cases L1 and L2, which do not account for minihaloes, we show predictions for minihalo-included cases by parametrizing the star formation inside minihaloes through $M_{*,\,\mathrm{III}}$ (mass of the Pop III star) and $J_{\mathrm{LW},\,\mathrm{th}}$ (threshold Lyman-Werner intensity). (Left) Late-overlap models. (Right) Early-overlap models.

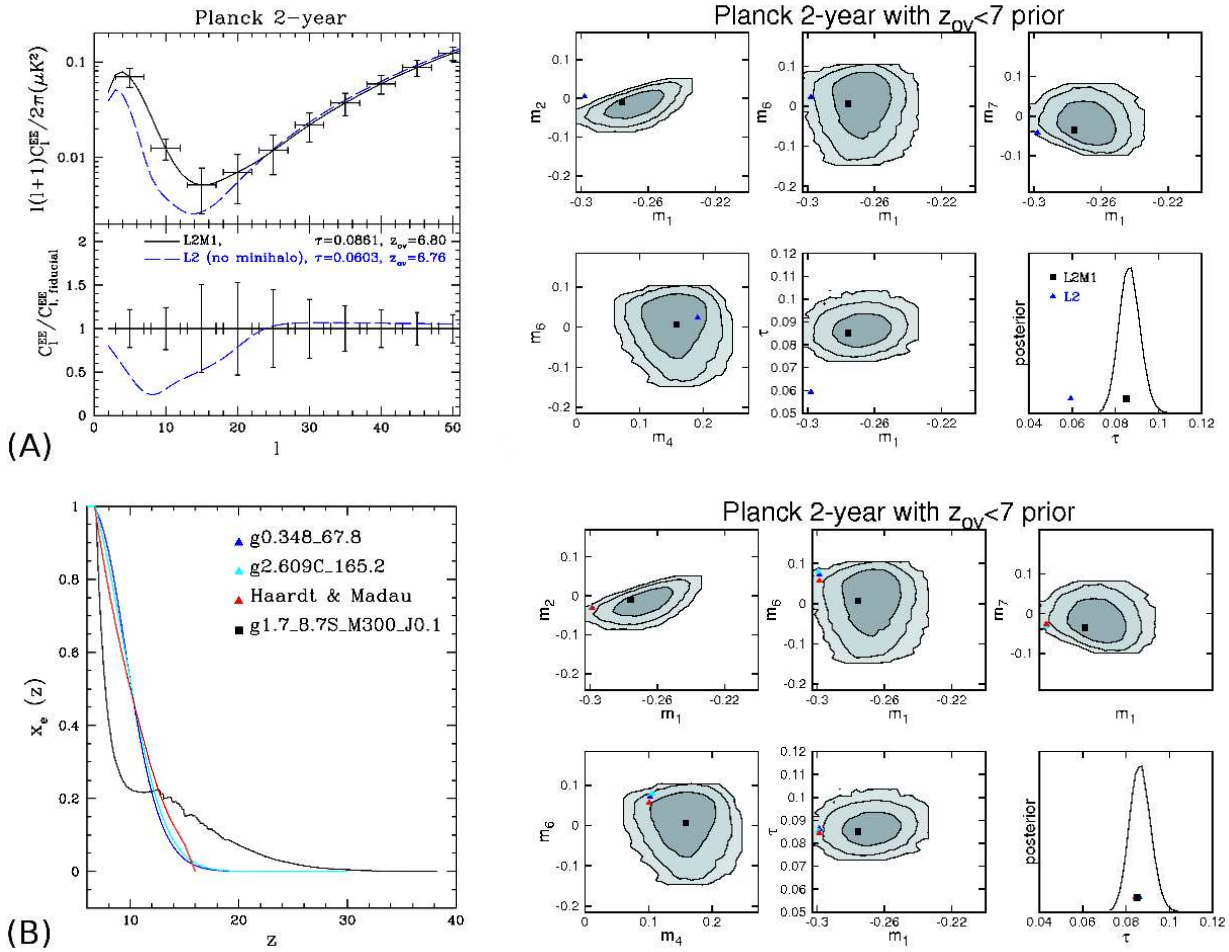

Fig. 4.— (A) Detecting the first stars. [*left*]: Forecasts of EE polarization power spectra of cases L2M1 (with minihaloes) and L2 (no minihaloes) for *Planck*. The error bars indicate the estimated *Planck* 2-year 1σ sensitivity including cosmic variance (top panel). Case L2M1 can be clearly distinguished from case L2. [*right*]: Model-selection power of *Planck*. Contours represent 1σ (68%), 2σ (95%) and 3σ (99.7%) confidence levels from inside out, on marginalized posterior distributions of selected parameters (m_μ's and $\tau_{\rm es}$) using mock data based upon Model L2M1 (black square). In each panel, values of m_μ for cases L2 and L2M1 are plotted. Case L2 (blue triangle) can be easily ruled out only from the measurement of $\tau_{\rm es}$ by *Planck*. The prior condition of $z_{\rm ov} \leq 7$ is applied here, which also rules out early reionization ($z_{\rm ov} \gtrsim 8$) models. (B) Breaking the degeneracy in $z_{\rm ov}$ and $\tau_{\rm es}$. [*left*]: Reionization histories of various reionization models, but with almost identical $z_{\rm ov}$ and $\tau_{\rm es}$. The model with minihalo sources (case L2M1, or $g1.7\_8.7S\_M300\_J0.1$, in black line) stands out from almost degenerate, no-minihalo models (in blue, cyan and red lines). [*right*]: Hypothesis-testing power of *Planck* on minihalo-included (black square) vs. no-minihalo models (triangles). Contours have the same meaning as those in (A). No-minihalo models are clustered and well separated from case L2M1 at $\gtrsim 2\sigma$ confidence level. The same color scheme for model specification is used in left and right panels – see legends in the left panel.